Neural tuning instantiates prior expectations in the human visual system

William J Harrison[1,2], Paul M Bays[3], & Reuben Rideaux[2,3,4]*

[1]School of Psychology, The University of Queensland, St Lucia, Australia

[2]Queensland Brain Institute, The University of Queensland, St Lucia, Australia

[3]Department of Psychology, The University of Cambridge, Cambridge, UK

[4]School of Psychology, The University of Sydney, Camperdown, Australia

*corresponding author: reuben.rideaux@sydney.edu.au

ABSTRACT

Perception is often modelled as a process of active inference, whereby prior expectations are combined with noisy sensory measurements to estimate the structure of the world. This mathematical framework has proven critical to understanding perception, cognition, motor control, and social interaction. While theoretical work has shown how priors can be computed from environmental statistics, their neural instantiation could be realised through multiple competing encoding schemes. Using a data-driven approach, here we extract the brain's representation of visual orientation and compare this with simulations from different sensory coding schemes. We found that the tuning of the human visual system is highly conditional on stimulus-specific variations in a way that is not predicted by previous proposals. We further show that the adopted encoding scheme effectively embeds an environmental prior for natural image statistics within the sensory measurement, providing the functional architecture necessary for optimal inference in the earliest stages of cortical processing.

INTRODUCTION

The human visual system is tasked with inferring environmental attributes from image data that can be corrupted by noise from both internal and external sources. To combat the influence of such noise, a statistically optimal, or ideal, observer would compute the distribution of possible environmental states, and combine this prior information with incoming sensory signals to infer the true state of a scene[1]. While this general framework for understanding sensory encoding is relatively uncontroversial, the biological instantiation of the prior for environmental statistics is largely mysterious.

Sensory representations are thought to be tuned to behaviourally relevant statistics of natural environments over evolutionary and developmental timescales[1–4]. As shown in **Figure 1a**, edges and contours in natural images are primarily oriented along the cardinal axes[5–8]. There is a corresponding anisotropy in the orientation selectivity of visual neurons in several mammalian species that prioritises the encoding of cardinally oriented information (**Fig. 1b**)[9–11]. Analogously, humans are superior on a range of visual tasks for stimuli that are oriented around cardinal orientations relative to oblique orientations [12]. Such biases in encoding and behaviour are even present in artificial intelligence systems trained on naturalistic movies[13,14]. Several computational accounts have attempted to unify the influence of environmental statistics on the properties of sensory neurons as well as perception[5,15,16], but have been unable to address empirically how such encoding is implemented at the neural level.

One way in which environmental regularities could be represented by biological systems is via sensory encoding schemes that allocate neural resources in relation to the natural frequency of various features. However, such models are consistent with multiple competing encoding schemes. In the domain of visual orientation, for example, biases in perception can be explained by corresponding biases in either the width *or* spacing of sensory tuning curves[5,15–18]. Therefore, while it is generally accepted that perceptual biases can be linked to anisotropies in environmental statistics, there is far less clarity about how these anisotropies are represented in the human visual system (as discussed in [19]). Moreover, leading models that account for cardinal biases in perception equate the prior probability of horizontal and vertical features[5,15,16], whereas earlier work suggests that horizontal features are over-represented relative to vertical[6,20]. These discrepancies may obfuscate a clear understanding of neural encoding schemes; we are not aware of any prior work that has attempted to link such biased environmental statistics with population-level responses of the human visual system. The way in which environmental priors are

represented in biological systems is a critical gap in our understanding of how the brain achieves optimal inference.

In the present study, we investigated the instantiation of environmental priors in the human visual system using electroencephalography (EEG) and inverted encoding models[21,22]. We developed novel neural decoding and generative modelling procedures with which to infer anisotropic coding in the human visual system, and compared these anisotropies with responses generated from encoding schemes with known neural response functions. Our approach therefore provides a generalisable means to test arbitrarily specified sensory encoding schemes. We show, however, that no previously proposed encoding scheme can explain the empirical neural data. Instead, we show that anisotropic neural responses can be explained almost entirely by a redistribution of sensory tuning curves that prioritises the most dominant environmental structure. We further show that the recovered neural code embeds a prior for natural image statistics within the sensory measurement, thereby simplifying the biological instantiation of optimal inference. Our results thus support the biological plausibility of perception as Bayesian inference by explaining how prior expectations are encoded by the tuning properties of sensory neurons.

RESULTS

Decoded neural responses over-represent horizontal. We recorded human observers' brain activity with EEG while they viewed rapidly presented oriented gratings (randomly sampled from a uniform distribution between 0-180°) and monitored for occasional changes in spatial frequency (**Fig. 2a**). Prior to the main analyses of the neural activity evoked by the gratings (**Fig. S1**), we established that orientation information was primarily represented in parietal and occipital EEG sensors (**Fig. S2**; *Method - Neural Decoding*); thus, we only included the signal from these 20 sensors in all subsequent analyses (inset of **Fig. 2b**, cyan dots). We first characterized orientation-related univariate activity. We sorted the gratings into six orientation bins (±15° around 0°, 30°, 60°, 90°, 120°, and 150°, where 0° is horizontal) and calculated the difference between the average evoked response for each bin from the grand average of responses, averaged over responses to all gratings. As shown in **Figure 2b**, there were significant differences in the response to orientations between approximately 50 to 400 ms following stimulus onset. The largest deviation from the mean response to all gratings was for horizontal orientations, which occurred in the initial stages of stimulus processing (50-100 ms following stimulus onset). We then collapsed the responses across time and calculated the average absolute response

82 for each grating orientation and found that response amplitude peaked around horizontal
83 gratings (**Fig. 2c**).

84 We next quantified temporal dynamics in orientation tuning using inverted encoding
85 analyses[21]. Using cross-fold validation, we trained and tested an inverted model using the
86 EEG signals to decode the orientation of each grating from the neural activity at each time
87 point. From the trial-by-trial decoded signals, we derived summary parameter estimates of
88 *accuracy* (the similarity between the decoded and presented stimulus orientation), *precision*
89 (the variability of decoded orientations within each bin), and *bias* (the average decoded
90 angle relative to the presented orientation; see *Method – Neural Decoding*).

91 The results from the neural decoding are shown in cyan in **Figure 3**. Accuracy of
92 decoded responses rose sharply from ~50 ms following stimulus onset and gradually
93 reduced over the following 400 ms (**Fig. 3a**, cyan data), revealing that decodable information
94 is relatively stable across time and robust to additional incoming information, i.e.,
95 subsequently presented stimuli, consistent with recent work[23,24]. We found a similar pattern
96 of results for the *precision* of decoded responses (**Fig. 3b**, cyan data), with precision
97 increasing sharply from ~50 ms and gradually reducing. Precision was significantly above
98 chance prior to stimulus presentation, likely because the decoder produced an over-
99 representation of some orientations, which is consistent with the anisotropic representation
100 of orientations shown in **Figure 2c**. As expected, we found no significant deviations in bias
101 when averaged across orientations (**Fig. 3c**, blue data). The orange data in **Figure 3** are
102 the results of a re-analysis of a previous study[23], which we will describe further in the
103 following section.

104 **Neural coding is highly anisotropic.** To quantify stimulus-specific variations in
105 neural representations, we measured accuracy, precision, and bias as a function of grating
106 orientation. To do so, we developed a novel inverted model analysis which returns these
107 parameter estimates for each of 180 unique grating stimuli (one for each orientation rounded
108 to the nearest degree; *Methods – Neural Decoding*). To maximize the signal-to-noise ratio
109 for each bin, we averaged results over the period in which there was above-chance accuracy
110 (50-450 ms), but the pattern of results is stable across different periods (**Fig. S3**).

111 Neural responses were strongly anisotropic, but not in a way predicted from any
112 leading model of neural coding[15,16]. For accuracy, we found a trimodal pattern of results
113 such that there was one large peak centered on horizontal and two smaller peaks positioned
114 around vertical (**Fig. 3d**). By contrast, we found a unimodal pattern of results for precision,
115 such that horizontal gratings were decoded most precisely (**Fig. 3e**). We found a sinusoidal

pattern of biases, comprising two attractive curves centered on the cardinal gratings (**Fig. 3f**). Although we found better orientation tuning and precision for horizontal orientations, the magnitude of the attractive biases was larger around the vertical than the horizontal gratings. A split-half analysis of the neural signals in the epoch used to decode orientation parameters confirmed this pattern of results was stable over the course of the epoch (**Fig. S3**).

To test the reproducibility of these results, we performed these analyses on a separate, previously published, dataset[23]. This prior study differed from our own in many aspects, such as the stimulus parameters, the observers' task, and the temporal design, which resulted in differences in the temporal dynamics of the decoded signal (as shown in **Figure 3a-c**, orange data). Despite these considerable differences across experiments, however, we found strikingly similar stimulus-specific variations in neural representations (**Fig. 3g-i**). Note that the observers' task in the previous study was to report whether grating stimuli were more cardinally or obliquely oriented on a given trial, likely resulting in increased precision around those orientations (**Fig. 3h**). This re-analysis therefore demonstrates that our neural decoding method is sensitive to task-related goals, with replicable estimates of orientation anisotropies in accuracy and bias.

Generative modelling of neural population responses. Previous theoretical work provides two primary variations in efficient encoding schemes to explain how anisotropies in orientation coding could be implemented at the neural level[5,15,16]. The proposed neural populations are instantiated such that either neurons tuned to cardinal orientations have narrower tuning (**Fig. 4a**, uneven tuning width) or that there are more neurons tuned to cardinal orientations (**Fig. 4a**, uneven tuning preference); however, these competing explanations cannot be resolved using behavioural measurements as they predict the same patterns of estimation error. To adjudicate between these population codes, therefore, we developed a novel generative modelling procedure to simulate EEG activity from neural tuning functions that had either isotropic tuning, or anisotropic tuning as specified by uneven tuning widths or uneven tuning preferences (*Methods – Generative Modelling*). We then applied the same inverted encoding analyses used on the empirical data to estimate accuracy, precision, and bias, as a function of orientation (**Fig. 4b**). While concerns have recently been raised about the extent to which inverted encoding analyses can be used to infer population representations[25–27], our novel generative modelling approach overcomes such issues by directly mapping the transformation of the output of a range of generative models to neural responses. A similar implementation has recently shown that such an approach is sensitive to changes in underlying population representations[28]. If either of the

150 hypothesised models of anisotropic orientation coding explains the true underlying neural
151 implementation, then the empirical data should match the decoded responses of the
152 simulated data from only a single generative population code.

153 We first generated neural responses from an unbiased isotropic bank of tuning
154 functions (**Fig. 4a**, even tuning). As expected, this simulation did not replicate the pattern of
155 results observed for the empirical data, as it produced a uniform pattern of accuracy,
156 precision, and biases across all orientations (**Fig. 5a**). We then generated neural responses
157 from an anisotropic bank of tuning functions specified by narrower tuning around the
158 cardinals (**Fig. 5b**). Although this population code produced a non-uniform distribution of
159 parameter estimates, the pattern of results did not match the empirical data: accuracy and
160 precision peaked around the obliques, not cardinals, and there was no clear pattern of
161 biases. Finally, we generated neural responses from tuning functions with orientation tuning
162 preferences clustered around the cardinals (**Fig. 5c**). The pattern of accuracy, precision,
163 and biases produced by this simulation captured the empirical results best out of the three
164 models tested: accuracy and precision peaked around cardinals, with modest attractive
165 biases. In contrast to the empirical results of the two datasets, however, the peak accuracies
166 and biases around horizontal and vertical orientations were equivalent, which was expected
167 from cardinally symmetric response functions, revealing that the modelled response
168 functions did not fully reflect the neural architecture underlying orientation anisotropies in
169 human visual cortex.

170 Neither of the proposed tuning schemes reproduced the empirical results. We
171 therefore exhaustively searched the space of cardinal and oblique tuning biases to test
172 which population code best explained the empirical data. We chose to manipulate tuning
173 preferences because the uneven tuning preference scheme provided the most promising
174 match to the empirical data (**Fig. 5c**). The modelled data and empirical data were compared
175 using their *discriminability*[29], a metric that considers the precision and bias – but not the
176 accuracy – of the decoded signal. We computed the similarity between the discriminability
177 of the empirical results and from data generated from population codes comprising all
178 possible combinations of horizontal and vertical biases (**Fig. 6a**), i.e., by independently
179 varying the clustering around horizontal and vertical orientations. We found that the model
180 that best described the empirical data was a population code with anisotropic cardinal
181 biases, where horizontals are 'more preferred' than verticals by a ratio of approximately 2:1.
182 These results are consistent with our univariate analyses (**Fig. 2**), and confirm that there is
183 an asymmetry between cardinal orientations, such that horizontals are more preferred than

verticals. Further, the ratio of horizontal to vertical asymmetry is consistent with previous estimates of the orientation content in natural visual scenes, but not human-made scenes[5].

A population code with uneven tuning preferences and an asymmetric cardinal anisotropy captured the empirical results well (**Fig. 6b**): this model reproduced the increased precision at horizontal orientations, and the sinusoidal pattern of biases with a larger attractive bias around vertical gratings. It also reproduced the trimodal distribution of accuracy, despite this metric not being used in the discriminability metric used in the fitting procedure. It is unclear, however, to what extent the redistribution of tuning curves around horizontal and vertical each influence the decoded pattern of anisotropic orientation representation; that is, which changes in accuracy, precision, and biases are related to the horizontal preference, and which are related to the vertical preference? To address this question, we generated EEG data from neural tuning functions with tuning preferences for horizontal orientations only (**Fig. 6c**). This simulation captured many of the phenomena observed in the empirical results: it recapitulated the increased accuracy and precision for horizontal gratings, and the asymmetric attractive biases around cardinal gratings. We did not expect a horizontal preference to capture the empirical patterns of results more closely than the classic symmetric cardinal preference models shown in **Figure 5b-c**.

A key diagnostic characteristic of the two empirical datasets is the reduction in accuracy for vertical orientations (**Fig. 3d, 3g**). This feature is only captured by a population code with asymmetric cardinal preferences (**Fig. 6b**). To understand why asymmetric cardinal preferences are critical to reproduce the accuracy around vertical orientations, we varied the noise level in the generative model. In the models presented above, we matched each population code to the signal-to-noise of the empirical data by titrating the noise injected into the simulated data (see *Method – Generative Modelling*). By reducing the noise level in the generative models, we can uncover the explanation for the reduction in accuracy around vertical: the reduced accuracy around vertical is due to a small repulsive bias (**Fig. S4**). This repulsive bias around vertical and the attractive bias around horizontal are additive, resulting in the appearance of a plateau in overall bias around vertical that can be seen in both empirical datasets (**Fig. 3f, 3i**) as well as the generated data (**Fig. 6b**), all of which include the influence of noise.

Joint coding of the prior and sensory measurement. A general solution to performing Bayesian inference involves embedding the prior *within* the sensory measurement[30–32]. In brief, if tuning curves are distributed such that their sum approximates the log of the prior, then the posterior is a linear readout of the population response,

simplifying the biological instantiation of optimal inference (full mathematical detail is given in *Method – Joint coding of the prior and sensory measurement*). We therefore compared how well the properties of the best-fitting population code, derived from our data-driven approach described above, capture environmental priors for natural and constructed scenes (**Fig. 7**). This analysis revealed that the sensory tuning curves do indeed embed the prior for natural image statistics (left panels, **Fig. 7**). The activity of the population code that best captures the responses of the human visual system therefore provides a stimulus representation from which a full (log) posterior can be computed through simple linear summation of activity, resulting in optimal inference in natural scenes. By comparison, the properties of the population code provide a poorer description of the prior for constructed scenes (right panels, **Fig. 7**).

DISCUSSION

We investigated whether the human visual system represents environmental attributes that are critical for optimal inference. Using our novel decoding analyses, we quantified surprising anisotropic neural responses that deviated from the expectations of leading models of visual prediction. By developing novel generative modelling tools, we were able to recover the underlying tuning properties of the population code driving the anisotropic neural responses. In addition to the cardinal anisotropy of orientation coding suggested by prior computational and behavioural investigations[5,15,16], we reveal that an asymmetry in cardinal representations is an inherent property of visual coding. Most importantly, our data provide the first clear evidence for a recent hypothesis about how priors are instantiated in biological systems[30]: the prior is embedded in the sensory measurement (**Figure 7**). By adjusting tuning curves to prioritise horizontal orientations and, to a lesser extent, vertical orientations, the early visual system implicitly combines the prior for natural images with incoming sensory signals. This coding scheme negates the need for the prior to be represented by a separate population of neurons, thereby improving neural efficiency.

The prioritisation of neural resources to horizontal orientations can be understood in the context of efficient coding[33]. A neural code is efficient if resources are allocated proportionally to the variation in the input signal along some feature dimension. While most prominent computational work models the anisotropic distribution of orientations as being symmetrical across cardinals, differences in horizontal and vertical contrast energy have been reported in measurements of natural image statistics[6,7] and a matching asymmetry has been observed in the tuning preferences of orientation-selective neurons[9–11]. For example, in a recent analysis of over 26,000 high quality digital photos of natural images, Harrison[7] reported that horizontal orientations were 10% more prevalent relative to vertical orientations. In an earlier analysis of 60 images, Hansen and Essock[20] found a similar over-representation of horizontal information across multiple spatial scales, suggesting the dominance of horizontal information is a scale invariant property of natural scenes. In their Bayesian account of visual orientation perception, Girshick et al.[5] derived estimates of observers' priors for orientation and found a close correspondence to cardinally-biased, but symmetric, environmental statistics. Close inspection of their results, however, shows that both the average of observers' recovered prior and the distribution of image statistics indicated greater representation of horizontal over vertical information, particularly in images of natural scenes (their data are re-plotted as the coloured traces in **Fig. 7**). A sensory population code that prioritises horizontal information over vertical, and cardinals over

263 obliques, can thus be interpreted as representing the true distribution of environmental
264 statistics derived from natural scenes. It is interesting to note that the sum of the tuning
265 curves provides a relatively poor approximation of the statistics of constructed scenes,
266 raising the possibility that the default tuning of sensory systems depends more on statistics
267 accumulated over evolutionary time scales than developmental time scales.

268 Linking anisotropies in orientation perception to neural tuning schemes is challenging
269 because behavioural measurements are confounded by response biases, which can be in
270 direct conflict with perceptual biases[34]. Here we avoided this confound by measuring biases
271 in the neural representation of passively viewed oriented gratings, and we then replicated
272 these effects using an independent dataset in which observers were actively engaging in a
273 visual discrimination task. A further advantage of our method is that it allowed us to directly
274 test, through generative modelling, the population level neural tuning properties that give
275 rise to anisotropies in the representation of orientation. The impact of this method is
276 highlighted by the inability of previous work to adjudicate between population codes
277 designed with uneven tuning preferences versus uneven tuning widths. Our results may
278 appear to contradict earlier neuro-imaging studies that found horizontal and vertical
279 orientations are equally over-represented in cortex relative to obliques[35]. However, close
280 inspection of these earlier data also reveals a clear horizontal/vertical asymmetry. It is
281 therefore likely that the assumption of equal cardinal responsiveness has led the
282 asymmetries we reveal to have been overlooked in more recent neuro-imaging
283 investigations[36,37].

284 Beyond providing a diagnostic marker for the underlying neural implementation of
285 orientation tuning in the human visual cortex, the reduced accuracy and small repulsive bias
286 around vertical gratings (**Fig. S4**) may explain previous inconsistencies in the behavioural
287 literature of perceptual cardinal biases. In particular, both attractive and repulsive perceptual
288 biases have been reported around the cardinal orientations, when measured using different
289 experimental paradigms[5,34,38]. This discrepancy has been explained within a Bayesian
290 framework as the result of either manipulating external (stimulus) or internal (neural) noise[16].
291 Under this framework, humans are assumed to have a prior distribution that gives
292 preference to cardinal orientations. Increasing external noise results in a greater reliance on
293 this prior (attraction towards cardinals), whereas increasing internal noise produces a bias
294 away from this prior (repulsion away from cardinals). Our findings show that there is small
295 repulsive bias around vertical, which is surrounded by a - considerably larger - attractive
296 bias. It is feasible that the smaller repulsive bias could be obscured by the larger attractive

bias under conditions of low signal-to-noise. Thus, this provides an alternative explanation for how manipulating noise could lead to observing either attractive or repulsive biases (at least around vertical orientations), which can be tested in future psychophysical investigations.

The neural responses recorded in the current study with EEG represent activity from primary visual cortex in addition to other upstream visual areas (e.g., V2). Thus, while we modelled the orientation tuning functions of neurons based on the known properties of V1 neurons, it is likely that other neurons within the visual processing cascade, which have more tuning properties, also contributed recorded representation. While neurophysiological work suggest similar orientation biases are present in higher visual regions, e.g., V5/MT[39], future work using an imaging technique with better spatial specificity, e.g., fMRI could test whether the same prior is instantiated across different cortical areas.

In summary, here we apply novel neural decoding and generative modelling approaches that reveal, replicate, and explain hitherto unknown aspects of sensory anisotropies. For the first time, we adjudicate between competing models of uneven neural tuning, demonstrating that uneven tuning preferences, but not tuning width, explain cardinal biases. We further show that anisotropies in the representation of orientation are almost entirely explained by a preference for horizontal orientations, while the smaller preference for vertical orientations produces a small repulsive bias that may account for previous discrepancies in attractive and repulsive cardinal bias. More broadly, we demonstrate both a new neural decoding algorithm and a corresponding generative modelling procedure that can be used in a principled manner to describe neural representations in high fidelity and explain their underlying architecture.

METHODS

Participants. Thirty-seven neurotypical human adults (mean±standard deviation age, 23.8±4.6 years; 23 females) participated in the experiment. Observers were recruited from The University of Queensland, had normal or corrected-to-normal vision (assessed using a standard Snellen eye chart), and were required to pass an initial screening session to qualify for the experiment (see *Stimuli, task, and procedure* Section for details). Data from one participant were omitted from analyses due to hardware failure. All participants were naïve to the aims of the experiment and gave informed written consent. The experiment was approved by The University of Queensland Human Research Ethics Committee.

Apparatus. The experiment was conducted in a dark, acoustically and electromagnetically shielded room. The stimuli were presented on a 24-inch ViewPixx monitor (VPixx technologies, Inc., Montreal) with 1920 x 1080 resolution and a refresh rate of 144 Hz. Viewing distance was maintained at 45 cm using a chinrest, meaning the screen subtended 61.18° x 36.87° (each pixel 2.4' x 2.4'). Stimuli were generated in MATLAB v2020a (The MathWorks, Inc., Matick, MA) using Psychophysics Toolbox[40,41] v3.0.18.13 (see http://psychtoolbox.org/). EEG signals were recorded using 64 Ag-AgCl electrodes (BioSemi, Amsterdam, Netherlands).

Stimuli, task, and procedure. The stimuli comprised sinewave gratings (1 cycle/°, 0.5 contrast, random phase) presented centrally within a circular aperture (radius 4.2°), which was smoothed at the edges, on a mid-grey background. A centrally positioned green fixation dot (radius 0.25°) was presented to reduce eye movements. To maintain attention, participants were instructed to count the number of 'target' stimuli, in which the spatial frequency of the grating was reduced (0.66 cycle/°). Between 0-3 targets appeared during each trial, selected at random.

Trials consisted of grating stimuli (orientations randomly selected between 0-180°) presented for .05 s each, separated by a blank 0.15 s inter-stimulus-interval (ISI) for 10 s (neural probe). The numbers 0-3 were then displayed on the screen and participants were given 2 s to indicate the number of targets presented, using the mouse (detection task). This was repeated 12 times per block. Participants performed 6 blocks of trials (~20 min), receiving feedback on their detection accuracy at the end of each block.

Prior to the main experiment, participants were required to pass an initial screening session in which they completed the same task but without EEG. To pass the screening, participants were required to perform above chance (25%) on the detection task. Further, they were required to show a significant repulsive bias on a separate orientation

reproduction task (assessed using a one-tailed *t*-test), which was related to data collected for a different study. This resulted in approximately half of the participants being screened out (32 due to insufficient repulsive bias, and 8 due to both insufficient repulsive bias and low detection task performance). Screening and experiment sessions were separated by a minimum of 24 h. Note that the individuals who were screened out are not included in the *Participants* section.

EEG. The EEG signals were digitised at 1024 Hz sampling rate with a 24-bit A/D conversion. The 64 active scalp Ag/AgCl electrodes were arranged according to the international standard 10–20 system for electrode placement[42] using a nylon head cap. As per BioSemi system design, the common mode sense and driven right leg electrodes served as the ground, and all scalp electrodes were referenced to the common mode sense during recording. Offline EEG pre-processing was performed using EEGLAB v2021.1[45] in accordance with best practice procedures[43,44]. The data were initially down-sampled to 512 Hz and subjected to a 0.5 Hz high-pass filter to remove slow baseline drifts. Using EEGLAB, electrical line noise was removed using *pop_cleanline.m with the following parameters: bandwidth=2; all channels; linefreqs=[50 100 150 200 250]; normSpectrum=0; p=0.01; pad=2; scanforlines=true; sigtype=channels; tau=100; winsize=4; winstep=4*. The *clean_artifacts.m*[45] function (default parameters) was used to remove bad channels (identified using Artifact Subspace Reconstruction), which were then spherically interpolated from the neighbouring electrodes. Only individual channels were removed and interpolated, no time periods were removed from the data. Data were then re-referenced to the common average before being epoched into segments around each neural probe stimulus (-0.25 s to 0.5 s from the stimulus onset). Systematic artefacts from eye blinks, movements and muscle activity were identified using semi-automated procedures in the SASICA toolbox [46] and regressed out of the signal.

Neural Decoding. To characterise sensory representations of the stimuli, we used an inverted modelling approach to reconstruct the orientation of the gratings from the EEG signal[22]. We make several advances in the application of our models that negate the recent concerns[25,26] about the validity of the properties of the recovered population code (see ***Generative Modelling*** section below*)*. A theoretical (forward) model was nominated that described the measured activity in the EEG sensors given the orientation of the presented grating. The forward model was then used to obtain the inverse model that described the transformation from EEG sensor activity to stimulus orientation. The forward and inverse models were obtained using a ten-fold cross-validation approach in which 90% of the neural

probe data were used to obtain the inverse model on which the remaining 10% were decoded. In our modelling, we assume that EEG sensor noise is isotropic across orientations and additive with the signal; while this assumption would be violated if there were a systematic relationship between orientation preference and anatomical location across participants, abundant evidence rules out such a relationship in human and non-human brains[9,47–49].

Similar to previous work[21], the forward model comprised six hypothetical channels, with evenly distributed idealized orientation preferences between 0° and 180°. Each channel consisted of a half-wave rectified sinusoid raised to the fifth power. The channels were arranged such that a tuning curve of any orientation preference could be expressed as a weighted sum of the six channels. The observed EEG activity for each presentation could be described by the following linear model:

$$\mathbf{B} = \mathbf{W}\mathbf{C} + \mathbf{E} \tag{1}$$

where $\mathbf{B}$ indicates the (*m* sensors × *n* presentations) EEG data, $\mathbf{W}$ is a weight matrix (*m* sensors × 6 channels) that describes the transformation from EEG activity to stimulus orientation, $\mathbf{C}$ denotes the hypothesized channel activities (6 channels × *n* presentations), and $\mathbf{E}$ indicates the residual errors.

To compute the inverse model, we estimated the weights that, when applied to the data, would reconstruct the underlying channel activities with the least error. In line with previous magnetencephalography work[24,50], when computing the inverse model, we deviated from the forward model proposed by [21] by taking the noise covariance into account to optimize it for EEG data, given the high correlations between neighbouring sensors. We then estimated the weights that, when applied to the data, would reconstruct the underlying channel activities with the least error. Specifically, $\mathbf{B}$ and $\mathbf{C}$ were demeaned such that their average over presentations equalled zero for each sensor and channel, respectively. The inverse model was then estimated using a subset of the data, selected through cross-fold validation (10 folds). The hypothetical responses of each of the six channels were calculated from the training data in each fold, resulting in the response row vector $\mathbf{c}_{train,i}$ of length n_{train} presentations for each channel i. The weights on the sensors $\mathbf{w}_i$ were then obtained through least squares estimation for each channel:

$$\mathbf{w}_i = \boldsymbol{B}_{train}\mathbf{c}_{train,i}^{\mathrm{T}}\left(\mathbf{c}_{\mathrm{train,i}}\mathbf{c}_{train,i}^{\mathrm{T}}\right)^{-1} \tag{2}$$

where $\boldsymbol{B}_{train}$ indicates the (m sensors × n_{train} presentations) training EEG data. Subsequently, the optimal spatial filter $\mathbf{v}_i$ to recover the activity of the ith channel was obtained as follows[50]:

$$\mathbf{v}_i = \frac{\widetilde{\sum}_i^{-1}\mathbf{w}_i}{\mathbf{w}_i^{\mathrm{T}}\widetilde{\sum}_i^{-1}\mathbf{w}_i} \tag{3}$$

where $\widetilde{\sum}_i$ is the regularized covariance matrix for channel i. Incorporating the noise covariance in the filter estimation leads to the suppression of noise that arises from correlations between sensors. The noise covariance was estimated as follows:

$$\widehat{\sum}_i = \frac{1}{n_{\text{train}} - 1}\boldsymbol{\varepsilon}_i\boldsymbol{\varepsilon}_i^{\mathrm{T}} \tag{4}$$

$$\boldsymbol{\varepsilon}_i = \mathbf{B}_{train} - \mathbf{w}_i\mathbf{c}_{train,i} \tag{5}$$

where n_{train} is the number of training presentations. For optimal noise suppression, we improved this estimation by means of regularization by shrinkage using the analytically determined optimal shrinkage parameter[50], yielding the regularized covariance matrix $\widetilde{\sum}_i$.

In the orientation focused analyses (**Fig. 3d-e**), we adapted a method recently introduced by [27], which uses sparsely distributed channels to produce a dense representation of channel responses. The standard inverted modelling approach typically involves training and testing a model using a relatively small number of channels (e.g., 6) to represent the entire spectrum of identities across a given feature (e.g., orientation). The 'enhanced inverted encoding model' (eIEM) method involves repeatedly computing the inverse model while rotating the forward model channel orientation preferences until each orientation is represented by a channel response (e.g., 180 channels, one for each orientation). The eIEM method was established using data with feature identities sampled from discrete bins (e.g., 0°, 30°, 60°, 90°, 120° and 150°), which determine: *a*) the number of channels used in each model (e.g., 6), and *b*) the number of feature identities from which predictions could be derived from the dense output (e.g., 6). By contrast, we presented observers with orientations sampled from a continuous uniform distribution of all orientations. Thus, we first sorted presentations into five orientation bins (0°, 36°, 72°, 108°, and 144°). After rotating channels to produce 180 channel responses for each presentation, we then binned the responses according to the original grating orientation (rounded to nearest the nearest degree); that is, the orientation of the presentation prior to binning. This allowed us to produce high-resolution model predictions for each orientation. We performed this analysis at each time point within the epoch, but to improve the signal of

the estimates we averaged predictions across time points when there was reliable decoding accuracy (50-450 ms following stimulus onset).

For each presentation, we decoded orientation by converting the channel responses to polar form:

$$z = \mathbf{c} \cdot e^{2i\boldsymbol{\varphi}} \tag{6}$$

and calculating the estimated angle:

$$\hat{\theta} = \frac{\arg(z)}{2} \tag{7}$$

where $\mathbf{c}$ is a vector of channel responses and $\boldsymbol{\varphi}$ is the vector of angles at which the channels peak (multiplied by two to project 180° orientation space onto the full 360° space). From the decoded orientations, we computed three estimates: *accuracy*, *precision*, and *bias*. Accuracy represented the similarity of the decoded orientation to the presented orientation[24], and was expressed by projecting the mean resultant (averaged across presentations of the same grating orientation) of the difference between decoded and grating orientations onto a vector with 0°:

$$\hat{r}_\theta = \mathrm{Re}[\bar{R}], \quad \bar{R} = \frac{1}{n}\sum_{j=1}^{n} \exp\left(\mathrm{i}\left(\hat{\theta}_j - \theta\right)\right) \tag{8}$$

Precision was estimated by calculating the angular deviation[51] of the decoded orientations within each orientation bin:

$$\hat{\sigma}_\theta = \sqrt{2(1 - |\bar{R}|)} \tag{9}$$

and normalized, such that values ranged from 0 to 1, where 0 indicates a uniform distribution of decoded orientations across all orientations (i.e., chance-level decoding) and 1 represents perfect consensus among decoded orientations:

$$\hat{p}_\theta = 1 - \frac{2\hat{\sigma}_\theta}{\sqrt{2}} \tag{10}$$

Bias was estimated by computing the circular mean of angular difference between the decoded and presented orientation:

$$\hat{b}_\theta = \arg\left(\bar{R}\right) \tag{11}$$

Prior to the main neural decoding analyses, we established the sensors that contained the most orientation information by treating time as the decoding dimension and obtaining inverse models for each sensor, using ten-fold cross-validation. This analysis revealed that orientation was primarily represented in posterior sensors (**Fig. S2**); thus, for all subsequent analyses we only included signals from the parietal, parietal-occipital, occipital, and inion sensors to compute the inverse model.

Generative Modelling. To characterise changes in neural tuning which might have given rise to the empirical results observed, we used inverted modelling to decode orientation from simulated EEG data produced by neural populations with either isotropic tuning or anisotropic tuning specified by differences in tuning preferences or tuning widths. Although the empirical EEG data comprises a time series of neural activity, we only simulated temporally static data as we were comparing this with the time averaged empirical data. Simulated data were produced by assuming variable weights between a bank of response curves, each of which represented the aggregate responses of neural populations with similar tuning, with different orientation preference (*n*=16) and EEG sensors (*m*=32). As with the forward model, the neural functions were arranged such that a tuning curve of any orientation preference could be expressed as a weighted sum of the 16 functions. Thus, for each simulated presentation, the EEG activity was computed as:

$$s_i = \mathbf{c}_{\boldsymbol{\theta}}\mathbf{w}_i + u \tag{12}$$

where s_i denotes the activity of sensor i, $\mathbf{c}_\theta$ indicates the set of tuning curves evaluated at orientation θ, $\mathbf{w}_i$ denotes the weights between the sensor i and the response functions, and u indicates Gaussian noise (s.d.=6). The noise level was selected to approximate the level of noise observed in the empirical results. Neural tuning consisted of von Mises functions (κ=2), normalized such that they ranged from 0 to 1. Neuron-to-sensor weights ($\mathbf{w}_i$) were randomly assigned from a uniform distribution between 0 and 1. This range was selected for simplicity. The variance in weights between the activity of subpopulations of neurons and EEG sensors in the brain is likely different, however, our simulations confirmed that modifying this range had no qualitative influence on the pattern of results. Uneven *tuning preferences* were modelled by shifting the neural tuning functions according to the sum of two von Mises derivative functions (κ=0.5) centered on 0° (amplitude=15) and 90° (amplitude=10), such that the maximum shift applied was 15°. This resulted in shifting the neural response functions towards the cardinals, with increased clustering around horizontal relative to vertical. Uneven *tuning widths* were modelled by narrowing the neural tuning functions according to the sum of two von Mises functions (κ=2) centered on 0° (amplitude=15) and 90° (amplitude=10), such that the maximum increase to κ was 15. This resulted in narrowing the neural response functions that preferred cardinal orientations, with increased narrowing around horizontal relative to vertical.

In line with the empirical experiment, the orientation of each simulated presentation was drawn from a uniform distribution between 1-180°. We simulated 3600 presentations

from the even and uneven neural response functions. We then applied the same analyses as used on the empirical data to estimate accuracy, precision, and bias as a function of orientation. The final presented results are the average of parameters estimated from 36 simulated datasets.

To find the orientation anisotropy that best captured the empirical neural data, we computed the difference (error) between the empirical data and data that was simulated using all possible combinations of cardinal and oblique neural tuning preferences. The error was calculated as the difference between the *discriminability* of the decoded orientations from empirical and simulated data. Discriminability combines measures of precision and bias to provide an index of how discriminable signals are at each orientation [29]:

$$d_\theta = \frac{\hat{\sigma}_\theta}{1 + \hat{b}'_\theta} \tag{13}$$

where $\hat{b}'_\theta$ is the change in bias at orientation θ, which we estimated as:

$$\hat{b}'_\theta \approx \frac{\hat{b}\left(\theta + \frac{\delta}{2}\right) - \hat{b}\left(\theta - \frac{\delta}{2}\right)}{\delta} \tag{14}$$

where δ indicates the size to the window of estimation (16°). The generative data was stochastic, due to the injected noise, so we calculated the error ten times for each model and used the average. Neural tuning preference anisotropies were produced in the same manner as described above, and the amplitude of the shift was independently varied around both horizontal (0°) and vertical (90°) orientations, from -45 to 45, in increments of 1, resulting in a total of 91×91=8281 models.

Joint coding of the prior and sensory measurement. Although there is general agreement that the brain combines prior information with sensory signals, the physiological implementation of such Bayesian inference is less clear[52–55]. In a population of *N* neurons with independent Poisson variability and tuning curves $f(\theta)$, the joint likelihood of the response of the population given a stimulus of orientation θ is:

$$P(\mathbf{r}|\theta) = \prod_n^N \frac{f_n(\theta)^{r_n}}{r_n!} e^{-f_n(\theta)} \tag{15}$$

where $\mathbf{r}$ is a vector containing each unit's spike count and r_n is the number of spikes for unit n. It is convenient for biological sensory systems to signal log probabilities so that joint (log) probabilities can be computed linearly, for example by summing spikes:

$$\log P(\mathbf{r}|\theta) = \sum_n^N r_n \log f_n(\theta) - \sum_n^N f_n(\theta) - \sum_n^N \log r_n! \tag{16}$$

Bayes' rule tells us that the posterior is computed by multiplying the likelihood, for example as computed above, with a prior, $P(\theta)$, and dividing by the marginal likelihood, $P(\mathbf{r})$. Using log probabilities, the formulation for computing the log-posterior can then be written as:

$$\log P(\theta|\mathbf{r}) = \sum_{n}^{N} r_n \log f_n(\theta) - \sum_{n}^{N} f_n(\theta) + \log P(\theta) + C_1 \tag{17}$$

where C_1 is a normalizing constant that does not depend on θ and can be ignored for purposes of comparing posterior probabilities or obtaining a *maximum a posteriori* (MAP) estimate. Estimating the posterior in this way would require at least three populations of neurons (or if, for example, the computations are performed via the weights of lateral connections, three sets of weights): one set to encode the stimulus, one to represent the prior, and another to decode the signal. As noted by Simoncelli[30], a more general solution to performing Bayesian inference involves embedding the prior into the sensory measurement by distributing the sensory tuning curves such that their sum is equal (up to an additive constant) to the log of the prior:

$$\textstyle\sum_n^N f_n(\theta) = \log P(\theta) + C_2. \tag{18}$$

In this case, the second and third terms of equation 13 cancel out, such that the full log-posterior distribution can be computed (up to an additive constant) as a simple linear function of the sensory measurement:

$$\log P(\theta|\mathbf{r}) = \sum_{n}^{N} r_n \log f_n(\theta) + C_3. \tag{19}$$

This solution is more efficient than encoding the prior in a separate population, requiring only two populations: one to encode the stimulus and another to obtain the linear readout over the population.

The equations above specify optimal inference for a population of spiking neurons, whereas we measured meso-scale activity across the scalp. On the assumption that the best fitting population code we recovered from the neural data is a linear transformation of the underlying neural activity, then if the prior is embedded in the sensory measurement Eq 18 should hold. Or equivalently,

$$e^{\sum_n^N f_n(\theta)} \propto P(\theta). \tag{20}$$

To test this, we fit the exponentiated sum of the best-fitting tuning curves in our study to the distribution of image statistics as measured by Girshick et al.[5] for natural scenes versus constructed scenes using two separate linear models. While the sum of the tuning

curves predicted both sets of image statistics (ps < .001), they almost perfectly recovered the statistics of natural scenes, accounting for 92% of the variation in natural scene statistics, while providing a poor fit to constructed scenes, accounting for only 46% of the variation in constructed scene statistics. The requirement that the exponentiated sum of the tuning curves is proportional to the prior, as specified by equation 20, is therefore met for natural image statistics. The recovered coding scheme of the human visual system thus embeds the prior in the sensory measurement, providing a concise means by which to perform optimal inference.

Re-analysis of published data. To test the reproducibility of our empirical results, we re-analyzed a dataset from a comparable, previously published, study from another laboratory [23]. This dataset comprised 32 channel EEG activity in response to viewing of uniformly sampled oriented gratings. In King and Wyart's[23] experiment, observers were presented eight rapidly presented (5 Hz) oriented gratings per trial and tasked with reporting whether the gratings were, on average, aligned more to the cardinal or oblique axes. In total, there were approximately 4800 presentations per participant, with 15 participants included; for a more detailed description of the experiment and data, see [23]. We received the preprocessed data from the authors, on which we performed the same inverted encoding analyses as used on the data from our experiment.

Statistical analyses. Statistical analyses were performed in MATLAB v2020a and CircStat Toolbox v1.12.0.0[56]. For analyses of differences in univariate responses and parameter estimates between orientations as a function of time, a cluster correction was applied to remove spurious significant differences. First, at each time point, the effect size of orientation was calculated. A repeated measures analysis of variance was applied to calculate the F statistic associated with orientation. Next, we calculated the summed value of these statistics (separately for positive and negative values) within contiguous temporal clusters of significant values. We then simulated the null distribution of the maximum summed cluster values using permutation (n=1000) of the orientation labels, from which we derived the 95% percentile threshold value. Clusters identified in the data with a summed effect-size value less than the threshold were considered spurious and removed.

Data Availability. The EEG data generated in this study have been deposited in the following OSF database: https://osf.io/5ba9y/. Source data are provided as a Source Data file.

Code Availability. Code has been deposited in GitHub (https://github.com/ReubenRideaux/Neural-tuning-instantiates-prior-expectations-in-the-human-visual-system).

REFERENCES

1. Geisler, W. S. Visual Perception and the Statistical Properties of Natural Scenes. *Annual review of psychology* **59**, 167–192 (2008).
2. Barlow, H. B. Single Units and Sensation: A Neuron Doctrine for Perceptual Psychology? *Perception* **1**, 371–394 (1972).
3. Burgess, A. E., Wagner, R. F., Jennings, R. J. & Barlow, H. B. Efficiency of human visual signal discrimination. *Science* **214**, 93–94 (1981).
4. Srinivasan, M. V., Laughlin, S. B. & Dubs, A. Predictive Coding: A Fresh View of Inhibition in the Retina. *Proceedings of the Royal Society B: Biological Sciences* **216**, 427–459 (1982).
5. Girshick, A. R., Landy, M. S. & Simoncelli, E. P. Cardinal rules: visual orientation perception reflects knowledge of environmental statistics. *Nat Neurosci* **14**, 926–932 (2011).
6. Hansen, B. C. & Essock, E. A. A horizontal bias in human visual processing of orientation and its correspondence to the structural components of natural scenes. *Journal of Vision* **4**, 5 (2004).
7. Harrison, W. J. Luminance and Contrast of Images in the THINGS Database: *Perception* **51**, 244–262 (2022).
8. Oliva, A. & Torralba, A. Modeling the Shape of the Scene: A Holistic Representation of the Spatial Envelope. *International Journal of Computer Vision* **42**, 145–175 (2001).
9. Fang, C., Cai, X. & Lu, H. D. Orientation anisotropies in macaque visual areas. *Proceedings of the National Academy of Sciences* **119**, e2113407119 (2022).
10. Roth, M. M., Helmchen, F. & Kampa, B. M. Distinct Functional Properties of Primary and Posteromedial Visual Area of Mouse Neocortex. *Journal of Neuroscience* **32**, 9716–9726 (2012).
11. Wang, G., Ding, S. & Yunokuchi, K. Difference in the representation of cardinal and oblique contours in cat visual cortex. *Neuroscience Letters* **338**, 77–81 (2003).
12. Appelle, S. Perception and discrimination as a function of stimulus orientation: The ‘oblique effect’ in man and animals. *Psychological Bulletin* **78**, 266–278 (1972).
13. Rideaux, R. & Welchman, A. E. But still it moves: Static image statistics underlie how we see motion. *J. Neurosci.* **40**, 2538–2552 (2020).
14. Rideaux, R. & Welchman, A. E. Exploring and explaining properties of motion processing in biological brains using a neural network. *Journal of Vision* **21**, 11 (2021).

15. Taylor, R. & Bays, P. M. Efficient Coding in Visual Working Memory Accounts for Stimulus-Specific Variations in Recall. *J. Neurosci.* **38**, 7132–7142 (2018).
16. Wei, X.-X. & Stocker, A. A. A Bayesian observer model constrained by efficient coding can explain 'anti-Bayesian' percepts. *Nat Neurosci* **18**, 1509–1517 (2015).
17. Fischer, B. J. Bayesian estimates from heterogeneous population codes. in *The 2010 International Joint Conference on Neural Networks (IJCNN)* 1–7 (2010). doi:10.1109/IJCNN.2010.5596687.
18. Ganguli, D. & Simoncelli, E. Implicit encoding of prior probabilities in optimal neural populations. in *Advances in Neural Information Processing Systems* vol. 23 (Curran Associates, Inc., 2010).
19. Maloney, R. T. & Clifford, C. W. G. Orientation anisotropies in human primary visual cortex depend on contrast. *NeuroImage* **119**, 129–145 (2015).
20. Hansen, B. C., Essock, E. A., Zheng, Y. & Deford, J. K. Perceptual anisotropies in visual processing and their relation to natural image statistics. *Network: Computation in Neural Systems* **14**, 501–526 (2003).
21. Brouwer, G. J. & Heeger, D. J. Decoding and reconstructing color from responses in human visual cortex. *Journal of Neuroscience* **29**, 13992–14003 (2009).
22. Brouwer, G. J. & Heeger, D. J. Cross-orientation suppression in human visual cortex. *Journal of Neurophysiology* **106**, 2108–2119 (2011).
23. King, J.-R. & Wyart, V. The Human Brain Encodes a Chronicle of Visual Events at Each Instant of Time Through the Multiplexing of Traveling Waves. *J. Neurosci.* **41**, 7224–7233 (2021).
24. Kok, P., Mostert, P. & de Lange, F. P. Prior expectations induce prestimulus sensory templates. *Proceedings of the National Academy of Sciences* **114**, 10473–10478 (2017).
25. Liu, T., Cable, D. & Gardner, J. L. Inverted Encoding Models of Human Population Response Conflate Noise and Neural Tuning Width. *J. Neurosci.* **38**, 398–408 (2018).
26. Gardner, J. L. & Liu, T. Inverted Encoding Models Reconstruct an Arbitrary Model Response, Not the Stimulus. *eNeuro* **6**, (2019).
27. Scotti, P. S., Chen, J. & Golomb, J. D. *An enhanced inverted encoding model for neural reconstructions*. 2021.05.22.445245 https://www.biorxiv.org/content/10.1101/2021.05.22.445245v2 (2021) doi:10.1101/2021.05.22.445245.
28. Rideaux, R., West, R. K., Rangelov, D. & Mattingley, J. B. Distinct early and late neural mechanisms regulate feature-specific sensory adaptation in the human visual system. *Proceedings of the National Academy of Sciences* **120**, e2216192120 (2023).

29. Wei, X.-X. & Stocker, A. A. Lawful relation between perceptual bias and discriminability. *Proceedings of the National Academy of Sciences* **114**, 10244–10249 (2017).

30. Simoncelli, E. P. Optimal Estimation in Sensory Systems. (2009) doi:10.7551/mitpress/8029.003.0046.

31. Ganguli, D. & Simoncelli, E. P. Efficient sensory encoding and Bayesian inference with heterogeneous neural populations. *Neural Computation* **26**, 2103–2134 (2014).

32. Rich, D., Cazettes, F., Wang, Y., Peña, J. L. & Fischer, B. J. Neural representation of probabilities for Bayesian inference. *J Comput Neurosci* **38**, 315–323 (2015).

33. Simoncelli, E. P. & Olshausen, B. A. Natural Image Statistics and Neural Representation. *Annu. Rev. Neurosci.* **24**, 1193–1216 (2001).

34. Tomassini, A., Morgan, M. J. & Solomon, J. A. Orientation uncertainty reduces perceived obliquity. *Vision Research* **50**, 541–547 (2010).

35. Furmanski, C. S. & Engel, S. A. An oblique effect in human primary visual cortex. *Nat Neurosci* **3**, 535–536 (2000).

36. van Bergen, R. S., Ji Ma, W., Pratte, M. S. & Jehee, J. F. M. Sensory uncertainty decoded from visual cortex predicts behavior. *Nat Neurosci* **18**, 1728–1730 (2015).

37. Roth, Z. N., Kay, K. & Merriam, E. P. Natural scene sampling reveals reliable coarse-scale orientation tuning in human V1. *Nat Commun* **13**, 6469 (2022).

38. de Gardelle, V., Kouider, S. & Sackur, J. An oblique illusion modulated by visibility: Non-monotonic sensory integration in orientation processing. *Journal of Vision* **10**, 6 (2010).

39. Xu, X. *et al.* Optical imaging of visually evoked responses in prosimian primates reveals conserved features of the middle temporal visual area. *Proceedings of the National Academy of Sciences* **101**, 2566–2571 (2004).

40. Brainard, D. H. The Psychophysics Toolbox. *Spatial Vision* **10**, 433–436 (1997).

41. Pelli, D. G. The VideoToolbox software for visual psychophysics: Transforming numbers into movies. *Spatial Vision* vol. 10 437–442 Preprint at https://doi.org/10.1163/156856897X00366 (1997).

42. Oostenveld, R. & Praamstra, P. The five percent electrode system for high-resolution EEG and ERP measurements. *Clinical Neurophysiology* 7 (2001).

43. Bigdely-Shamlo, N., Mullen, T., Kothe, C., Su, K.-M. & Robbins, K. A. The PREP pipeline: standardized preprocessing for large-scale EEG analysis. *Frontiers in Neuroinformatics* **9**, (2015).

677 44. Keil, A. *et al.* Committee report: Publication guidelines and recommendations for studies using
678 electroencephalography and magnetoencephalography. *Psychophysiology* **51**, 1–21 (2014).
679 45. Delorme, A. & Makeig, S. EEGLAB: an open source toolbox for analysis of single-trial EEG dynamics
680 including independent component analysis. *Journal of Neuroscience Methods* **134**, 9–21 (2004).
681 46. Chaumon, M., Bishop, D. V. M. & Busch, N. A. A practical guide to the selection of independent
682 components of the electroencephalogram for artifact correction. *Journal of Neuroscience Methods* **250**,
683 47–63 (2015).
684 47. Roth, Z. N., Heeger, D. J. & Merriam, E. P. Stimulus vignetting and orientation selectivity in human visual
685 cortex. *eLife* **7**, e37241 (2018).
686 48. Larsson, J. & Heeger, D. J. Two Retinotopic Visual Areas in Human Lateral Occipital Cortex. *J. Neurosci.*
687 **26**, 13128–13142 (2006).
688 49. De Valois, R. L., William Yund, E. & Hepler, N. The orientation and direction selectivity of cells in macaque
689 visual cortex. *Vision Research* **22**, 531–544 (1982).
690 50. Mostert, P., Kok, P. & de Lange, F. P. Dissociating sensory from decision processes in human perceptual
691 decision making. *Sci Rep* **5**, 18253 (2015).
692 51. Zar, J. H. *Biostatistical analysis*. (Pearson Education India, 1999).
693 52. Georgopoulos, A. P., Schwartz, A. B. & Kettner, R. E. Neuronal Population Coding of Movement Direction.
694 *Science* **233**, 1416–1419 (1986).
695 53. Jazayeri, M. & Movshon, J. A. Optimal representation of sensory information by neural populations. *Nat*
696 *Neurosci* **9**, 690–696 (2006).
697 54. Ma, W. J., Beck, J. M., Latham, P. E. & Pouget, A. Bayesian inference with probabilistic population codes.
698 *Nat Neurosci* **9**, 1432–1438 (2006).
699 55. Pouget, A., Dayan, P. & Zemel, R. S. Inference and Computation with Population Codes. *Annual Review*
700 *of Neuroscience* **26**, 381–410 (2003).
701 56. Berens, P. CircStat: A MATLAB Toolbox for Circular Statistics. *J. Stat. Soft.* **31**, (2009).
702

Acknowledgements

We thank Valentin Wyart and Jean-Remi King for sharing their data. This work was supported by an Australian Research Council Discovery Early Career Researcher Award to RR (DE210100790) and Wellcome Trust Senior Fellowship to PMB (106926).

Author Contributions Statement

RR contributed to conceptualization, methodology, software, formal analysis, investigation, data collection, data curation, visualization, project administration, and writing – original draft and revisions. WJH contributed to conceptualization, methodology, investigation, and writing – original draft and revisions. PMB contributed to methodology and writing – revisions.

Competing Interests Statement

The authors declare no competing interests.

Figure Captions

Figure 1. Neural tuning anisotropies mirror natural image statistics. a) Example image of natural scene (left) and its composite orientations (right). Orientations are coloured according to inset colour wheel; summary of relative orientation distribution indicated by inset histogram. b) Distribution of orientation selectivity in primary visual cortex of mouse[10], cat[11], and macaque[9]. Beach photo credit: Matthew Brodeur, https://unsplash.com/photos/DH_u2aV3nGM.

Figure 2. Anisotropic univariate neural responses evoked by oriented gratings. a) Schematic showing the experimental design; observers viewed rapidly presented oriented gratings (neural probe) while monitoring for target gratings with lower spatial frequency. Following the neural probe, participants indicated the number of target gratings detected using the mouse. b) Difference in event related potentials for gratings within orientation bins ([0°, 30°, 60°, 90°, 120°, 150°] ±15°) from the grand average of responses, averaged over responses to all gratings. Signals averaged across parietal and occipital EEG sensors (blue dots on topographic map) and participants (n=36). Orientation bin indicated in colour; event-locked and subsequent gratings indicated by solid and dashed black rectangles, respectively, and cluster-corrected periods of significant difference between orientations indicated by horizontal black bars. c) Time-averaged absolute signal amplitude for each grating orientation, binned to the nearest whole degree. The black line indicates the moving averages of data points.

Figure 3. Anisotropies in the neural representation of orientation revealed by inverted encoding. Average a) accuracy, b) precision (normalized decoding variability of decoded orientations, from 0 [uniform distribution] to 1 [no variability]), and c) bias of orientations decoded from neural responses. Cyan and orange lines indicate data from our experiment and from a previously published study[23], respectively. Shaded error bars in (a-b) and (c) indicate SEM and CI_{95}, respectively; coloured horizontal bars indicate cluster corrected periods that showed a significant difference from chance; horizontal dashed lines indicate chance-level. Note that this difference was significant for the entire period displayed in (b). d-f) The time-averaged (d) accuracy, (e) precision, and (f) bias of the inverted model responses, at all orientations, calculated from data collected in our experiment. Cyan lines in (d-f) indicate moving averages of data points (semi-transparent cyan dots). g-i) Same as (d-f), but calculated from previously published data [23].

Figure 4. Generative modelling of anisotropic neural tuning properties. a) Neural response functions for a population of orientation tuned neurons. Neurons may have even tuning properties across all orientations (even tuning), but theoretical work suggests that the anisotropies in orientation perception are either explained by denser clustering (uneven tuning preference) or narrower tuning (uneven tuning width) of neurons around cardinal orientations. Horizontally distributed black dots indicate tuning preferences. b) Illustration of the generative modelling procedure used to simulate neural data to test hypotheses of cardinal biases. A bank of orientation tuned neurons are connected to EEG sensors via random weights. We simulate EEG activity in response to multiple oriented gratings and then decode the orientation using inverted encoding. From the decoded orientations we calculate accuracy, precision, and bias parameters.

Figure 5. Standard encoding schemes produce anisotropic neural representations of orientation, but do not explain the empirical data. a-c) Results of simulations using neural response functions with (a) even or uneven (b) width, (c) or preference. The left column shows the neural response functions from which data were derived. The columns to the right are the parameter estimate results. Dark grey lines indicate moving averages of data points (semi-transparent dots). Blue insets show the corresponding moving averages from the empirical data; horizontally distributed black dots in the left panels indicate tuning preferences.

Figure 6. Horizontal preferences explain orientation anisotropies in human visual cortex. a) Difference (error) in discriminability (see *Methods – Generative Modelling* for detailed description) between empirical and simulated data as a function of horizontal and vertical clustering in the generative population code; less error indicates greater similarity between empirical and simulated data. The black outline indicates the region with the lowest 5% of error, and the white dashed circles indicate the position of the example population codes shown on the right. The red dotted circle indicates the position of the best fitting model (4). Results of simulations using neural response functions with (b) asymmetric cardinal tuning preferences and (c) unimodal horizontal tuning preference. The left column shows the neural response functions from which data were derived. The columns to the right are the parameter estimate results. Dark grey lines indicate moving averages of data points (semi-transparent dots). Blue insets show the corresponding moving averages from the empirical data; horizontally distributed black dots in the left panels indicate tuning preferences.

Figure 7. The redistribution of tuning curves effectively embeds a prior for natural image statistics in the sensory measurement. a) Horizontal-biased population code that best explained the neural responses, as described in Results. b-c) The left and right plots show the match of the properties of this population code with the distribution of orientation statistics for natural scenes (b) and constructed scenes (c) as measured by Girshick et al. (2011). In each plot, the coloured trace shows the probability of each orientation in a set of images, while the black trace shows the exponentiated sum of the best fitting tuning functions recovered from our generative model. Extending theory developed by Simoncelli (2009), the exponentiated sum of the tuning curves is proportional to the prior for natural scenes: $\exp(\sum_n f_n(\theta)) \propto P(\theta)$. Assuming Poisson neural variability, this allows the log posterior to be obtained as a weighted sum of the neural responses: $\log P(\theta|\mathrm{r}) = \sum_n r_n \log f_n(\theta) + const.$, providing an efficient means by which to perform optimal inference in the human visual system. Beach photo credit: Matthew Brodeur, https://unsplash.com/photos/DH_u2aV3nGM. City street photo credit: Andrea Cau, https://unsplash.com/photos/nV7GJmSq3zc.

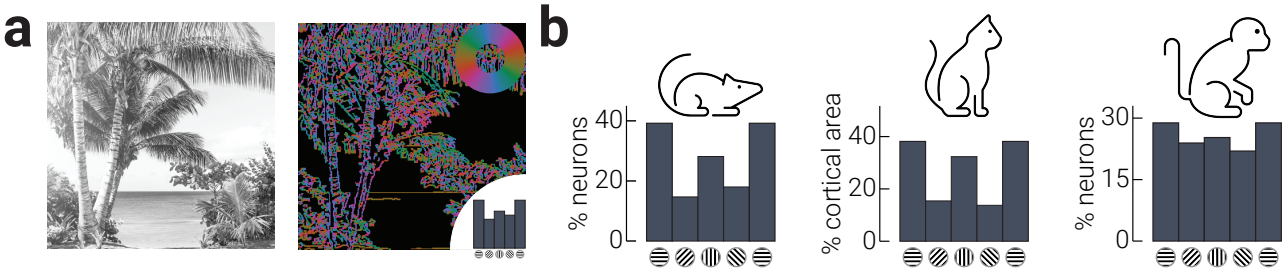
a
b
% neurons
40
20
0
% cortical area
40
20
0
% neurons
30
15
0

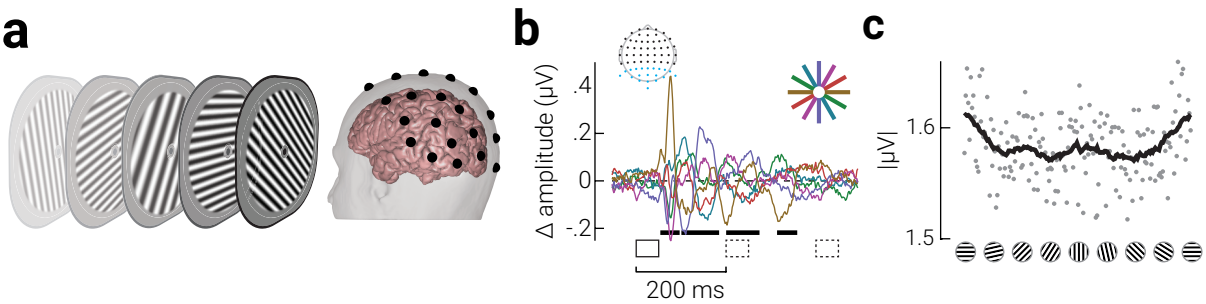
a
b
c
Δ amplitude (μV)
.4
.2
0
-.2
200 ms
|μV|
1.6
1.5

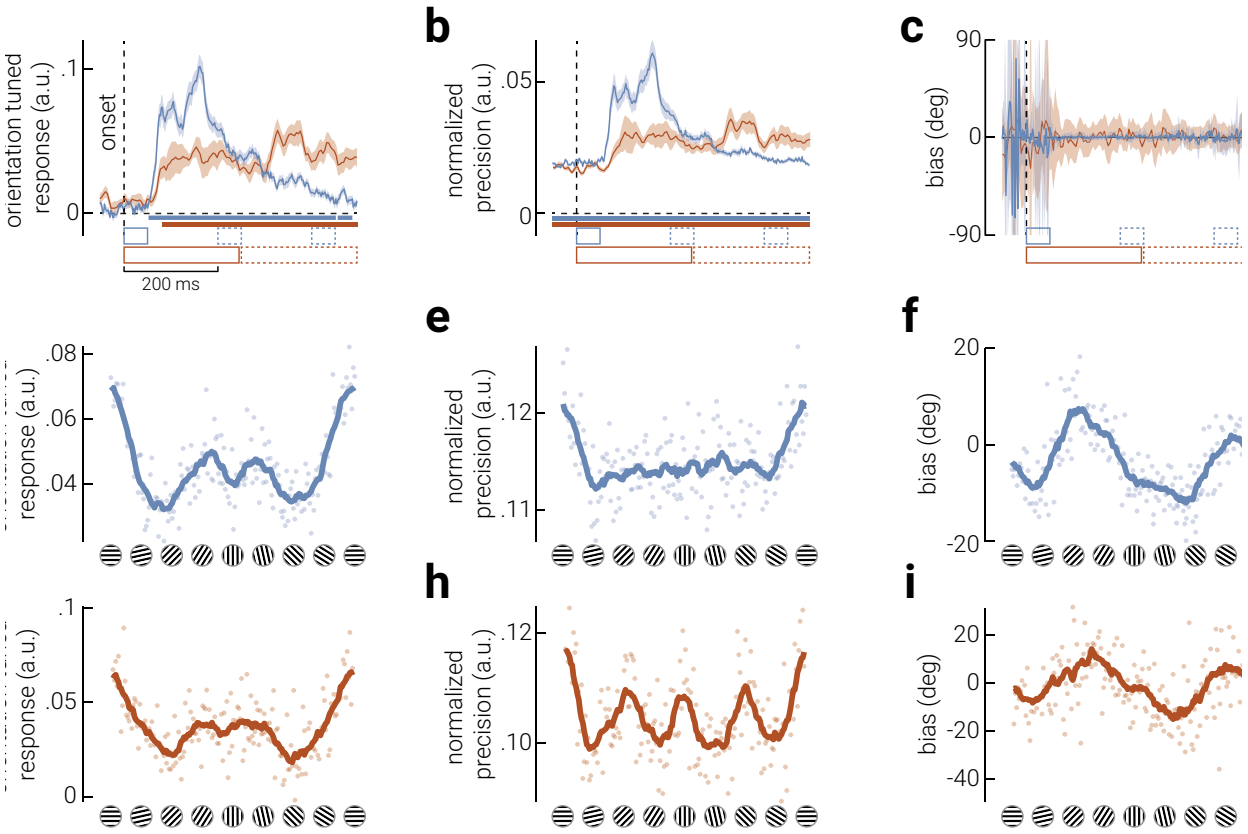
b
c
e
f
h
i
orientation tuned response (a.u.)
onset
.1
0
200 ms
normalized precision (a.u.)
.05
0
bias (deg)
90
0
-90
response (a.u.)
.08
.06
.04
.12
.11
20
0
-20
.1
.05
0
.12
.10
20
0
-20
-40

791

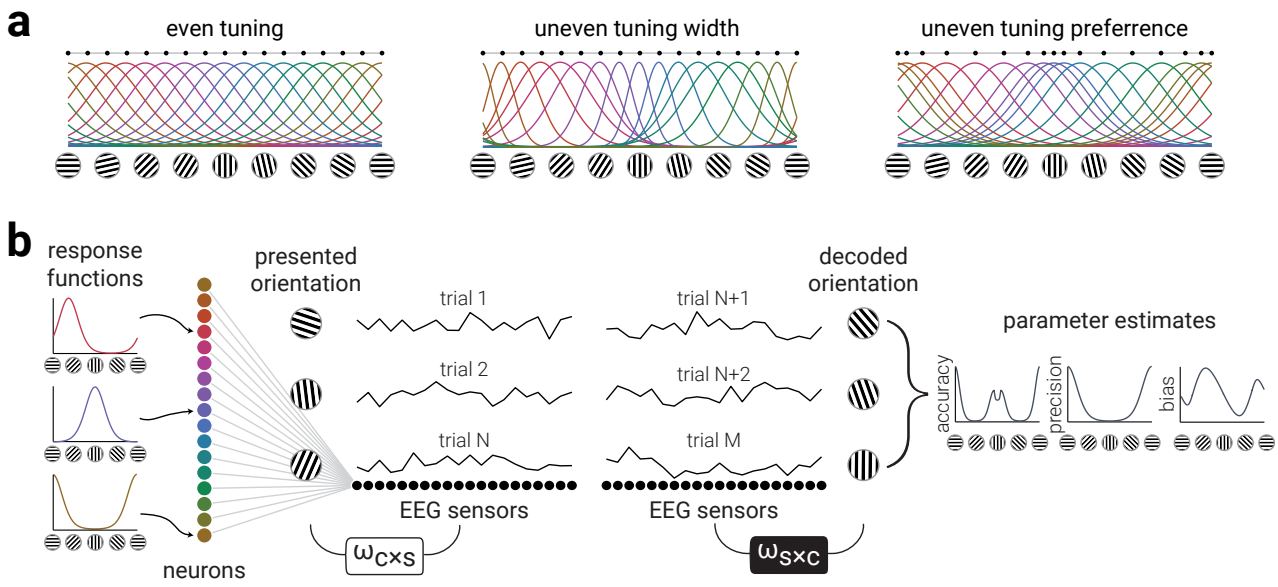
a
even tuning
uneven tuning width
uneven tuning preferrence
b
response functions
presented orientation
trial 1
trial 2
trial N
trial N+1
trial N+2
trial M
decoded orientation
parameter estimates
accuracy
precision
bias
EEG sensors
EEG sensors
neurons
ωC×S
ωS×C

792

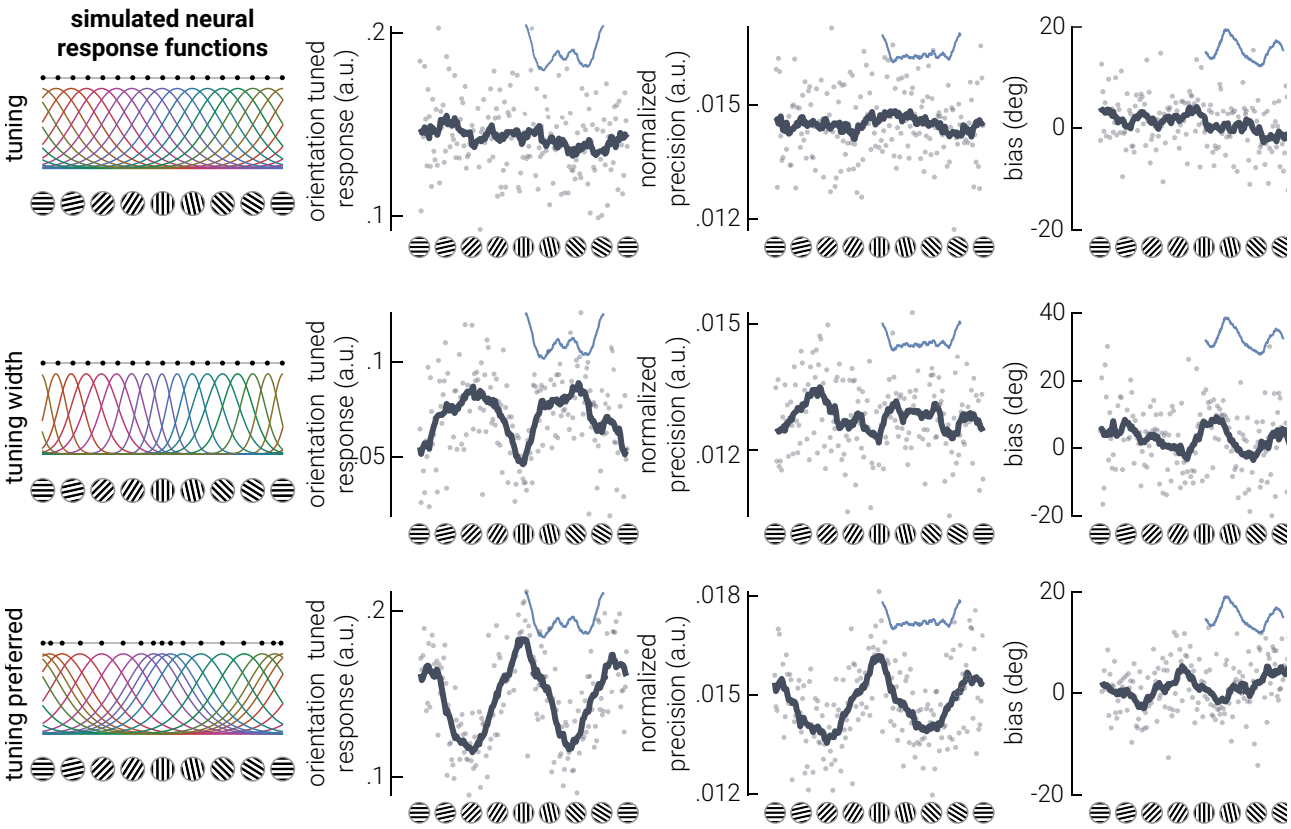
simulated neural response functions
tuning
tuning width
tuning preferred
orientation tuned response (a.u.)
.2
.1
.05
normalized precision (a.u.)
.018
.015
.012
bias (deg)
40
20
0
-20

793

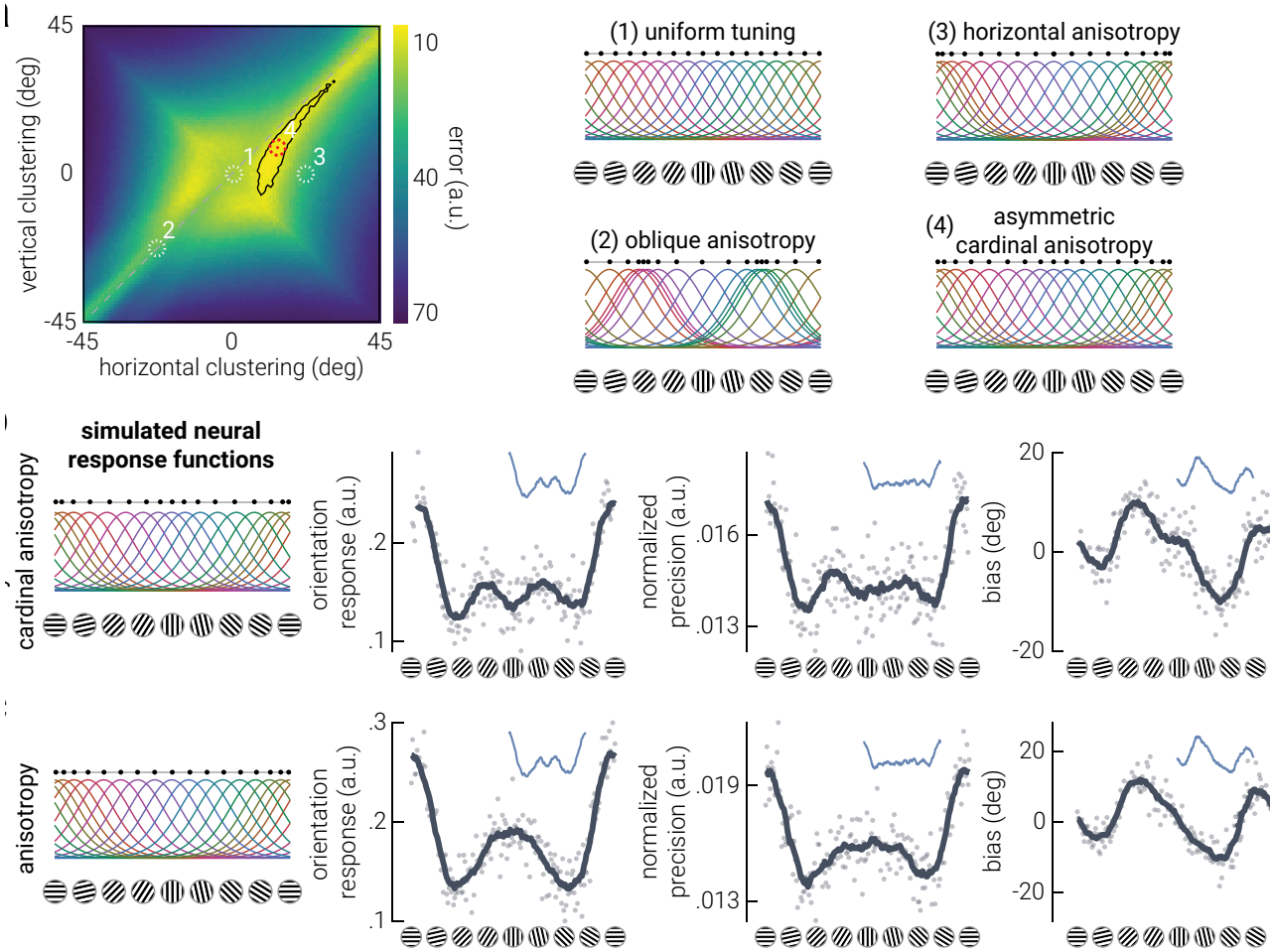
45
0
-45
-45
0
45
vertical clustering (deg)
horizontal clustering (deg)
1
2
3
10
40
70
error (a.u.)
(1) uniform tuning
(2) oblique anisotropy
(3) horizontal anisotropy
(4) asymmetric cardinal anisotropy
simulated neural response functions
cardinal anisotropy
anisotropy
orientation response (a.u.)
.3
.2
.1
normalized precision (a.u.)
.019
.016
.013
bias (deg)
20
0
-20

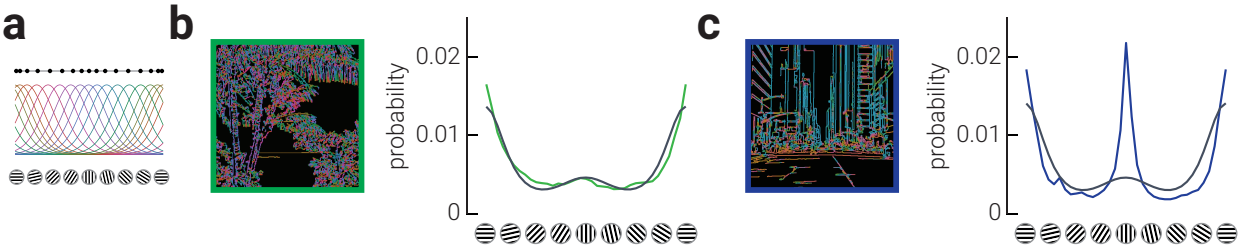
a
b
c
probability
0.02
0.01
0
probability
0.02
0.01
0

Supplementary Information

Neural tuning instantiates prior expectations in the human visual system

William J Harrison, Paul M Bays and Reuben Rideaux

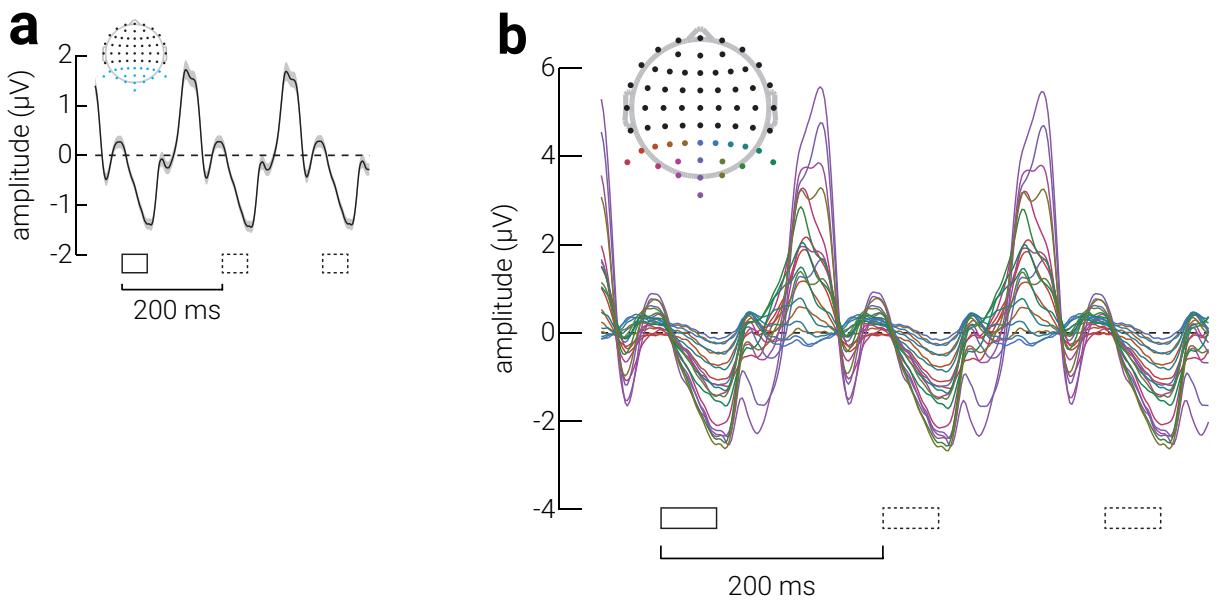

Figure S1. Event-related potentials. a) Grand average event-related potential, averaged across occipital and parietal sensors (cyan dots of inset), trials, and participants for the stimulus epoch (-50 to 500 ms). Event-locked and subsequent gratings indicated by solid and dashed black rectangles, respectively. **b**) Same as (**a**), but separately for each sensor (coloured dots of inset indicate sensor locations). Shaded regions in (**a**) indicate SEM across participants.

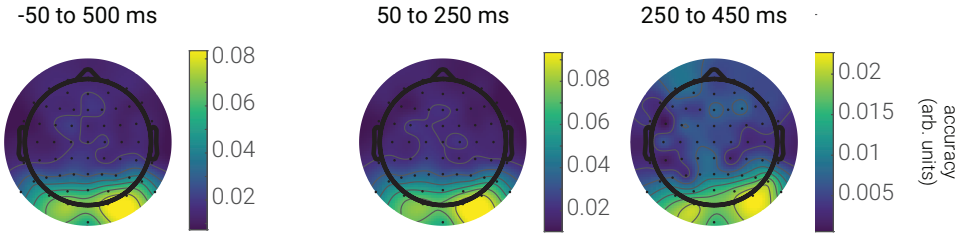

Figure S2. Topographic multivariate responses to orientations. Topographic accuracy, averaged across orientation for either the entire epoch (-50 to 500 ms), early in the epoch (50 to 250 ms) or late in the epoch (250 to 450 ms).

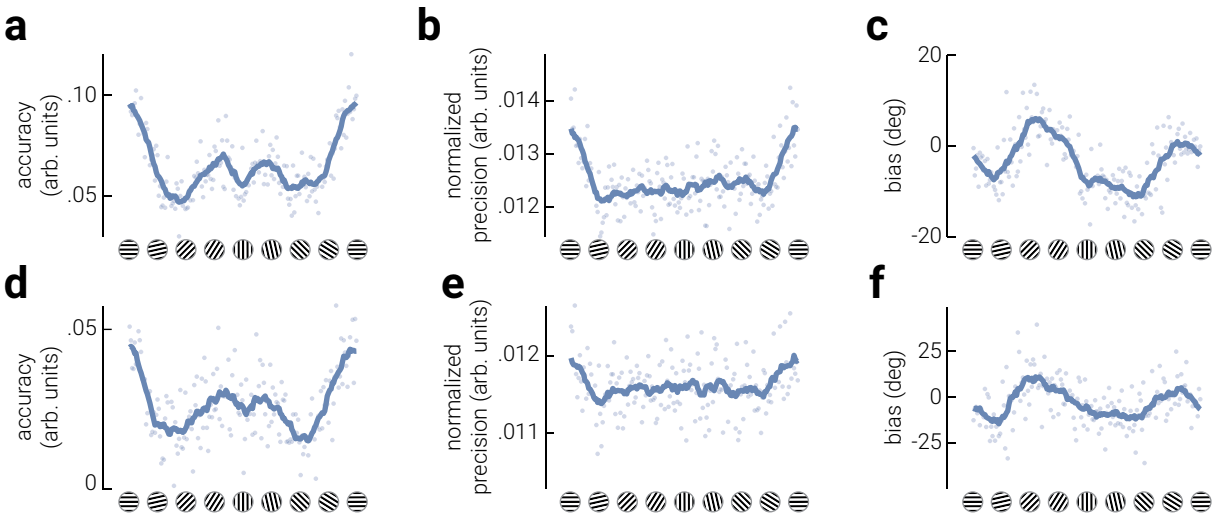

Figure S3. Temporal stability of anisotropies in the neural representation of orientation. a-c) The time-averaged (**a**) accuracy, (**b**) precision, and (**c**) bias of the inverted model responses, at all orientations, calculated from neural responses between 50 – 250 ms following stimulus onset. Cyan lines in indicate moving averages of data points (semi-transparent cyan dots). **d-f**) Same as (**a-c**), but calculated from neural responses between 250 – 450 ms following stimulus onset.

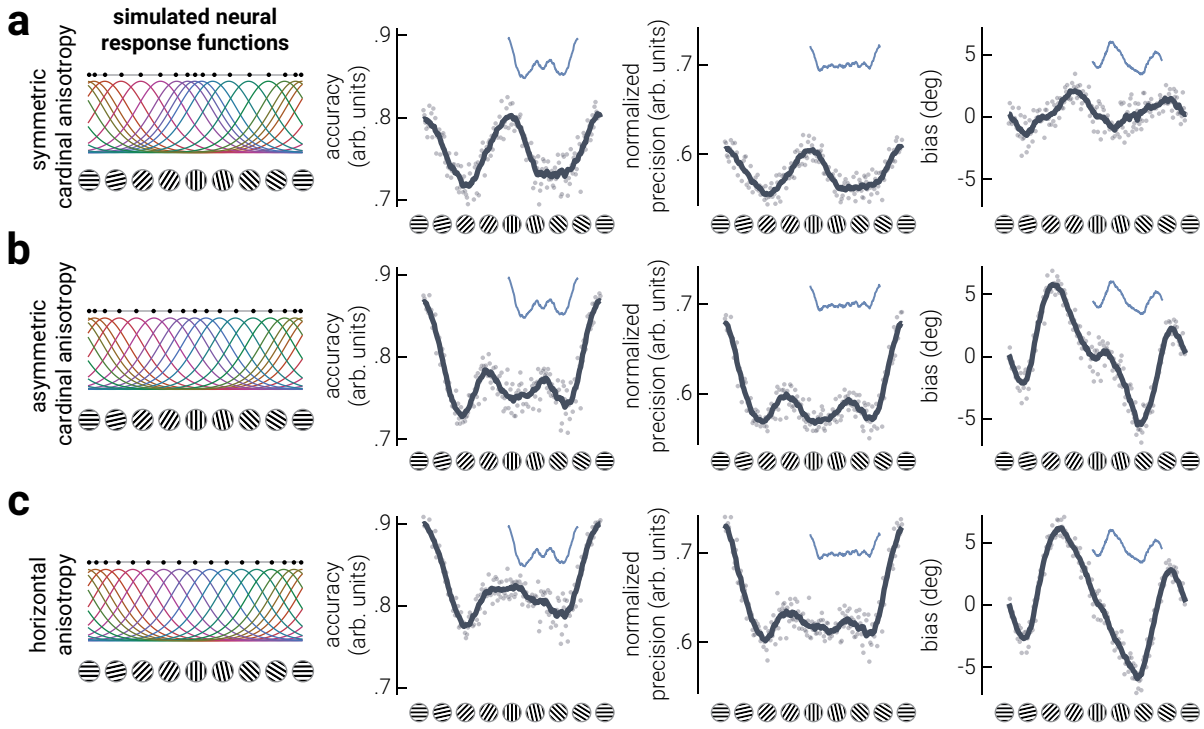

Figure S4. The influence of asymmetric cardinal tuning preferences when neural responses have high signal-to-noise. In our main simulations, we titrated the noise in the data to achieve similar signal-to-noise in the parameter estimates as in the empirical data. To reveal phenomena that may have been obscured by noise, here we reran the simulations with less noise. Results of simulations using neural response functions with (**a**) a symmetric cardinal anisotropy, (**b**) an asymmetric cardinal anisotropy, or (**c**) a horizontal anisotropy. The columns to the right are the parameter estimate results. Dark grey lines in indicate moving averages of data points (semi-transparent dots). Blue insets show the corresponding moving averages from the empirical data; horizontally distributed black dots indicate tuning preferences.